

The spatial distribution of circumstellar material of the wind-fed system GX 301-2

Xueying Zheng,^{1,2*} Jiren Liu,^{1†} Lijun Gou^{1,2}

¹Key Laboratory for Computational Astrophysics, National Astronomical Observatories, Chinese Academy of Sciences, Datun Road A20, Beijing 100012, China

²School of Astronomy and Space Sciences, University of Chinese Academy of Sciences, Datun Road A20, Beijing 100049, China

Accepted XXX. Received YYY; in original form ZZZ

ABSTRACT

The distribution of the circumstellar material in systems of supergiant X-ray binaries (SgXBs) is complex and not well probed observationally. We report a detailed study of the spatial distribution of the Fe K α -emitting material in the wind-fed system GX 301-2, by measuring the time delay between the Fe K α line and the hard X-ray continuum (7.8–12 keV) using the cross-correlation method, based on *XMM-Newton* observation. We found that to obtain the true time delay, it is crucial to subtract the underlying continuum of the Fe K α line. The measured size of the Fe K α -emitting region over the whole observation period is 40 ± 20 light-seconds. It is 5 times larger than the accretion radius estimated from a quasi-isotropic stellar wind, but consistent with the one estimated from a tidal stream, which could be the dominant mass-loss mechanism of GX 301-2 as inferred from the orbital distribution of the absorption column density previously. The measured time delay of the quiescent period is a little smaller than those of the flare periods, revealing the unsteady behaviour of the accretion flow in GX 301-2. Statistical and detailed temporal studies of the circumstellar material in SgXBs are expected for a large sample of SgXBs with future X-ray missions, such as Athena and eXTP.

Key words: Accretion neutron star: individual: GX 301-2 (SWIFT J1226.6-6244) – X-rays: binaries – circumstellar matter – stars: winds, outflows

1 INTRODUCTION

In systems of supergiant X-ray binaries (SgXBs), the compact star (either neutron star or black hole) accretes the wind material from its massive companion star and emits strong X-ray radiation (Martínez-Núñez et al. 2017). The compact star produces a bow shock in the surrounding material and is trailed by an accretion wake (e.g. Davidson & Ostriker 1973). The accretion flow in such a binary system is generally unsteady as shown in numerical simulations (e.g. Taam & Fryxell 1988; Blondin et al. 1990). The circumstellar material can be probed by the soft X-ray absorption of the intrinsic X-ray emission (e.g. Nagase 1989). The orbital distribution of the absorption column density of some sources, such as 4U 1700-37, requires an additional tidal stream (Haberl et al. 1989). In the case of GX 301-2, a classical SgXB, the modeled mass-loss rate of

the stream exceeds that in the stellar wind, thus the tidal stream can dominate the evolution of the massive companion star (Leahy & Kostka 2008). The spatial distribution of the circumstellar material can be probed with X-ray fluorescence lines, which are produced when the surrounding material reprocesses the intrinsic hard X-ray emission of the compact star. The most prominent fluorescence feature is the Fe K α line at 6.4 keV, which is a hallmark of SgXBs (Torrejón et al. 2010; Giménez-García et al. 2015).

There are several ways to constrain the material distribution surrounding the compact star with the observed Fe K α line. The line width of the Fe K α line can be used to constrain the size of the Fe K α -emitting region. The measured line widths using *Chandra* high-energy transmission grating spectrometer (HETG) are within 400 and 4000 km s⁻¹, indicating sizes from 10⁹ to 10¹¹ cm, if assuming the Fe K α -emitting gas is virialize (Tzanavaris & Yaqoob 2018). For eclipsing SgXBs, the decrease of the Fe K α fluxes during the eclipse can be used to infer the Fe K α -emitting region. It was found that the bulk of the Fe K α line originates

* E-mail: zhengxy@nao.cas.cn

† E-mail: jirenliu@nao.cas.cn

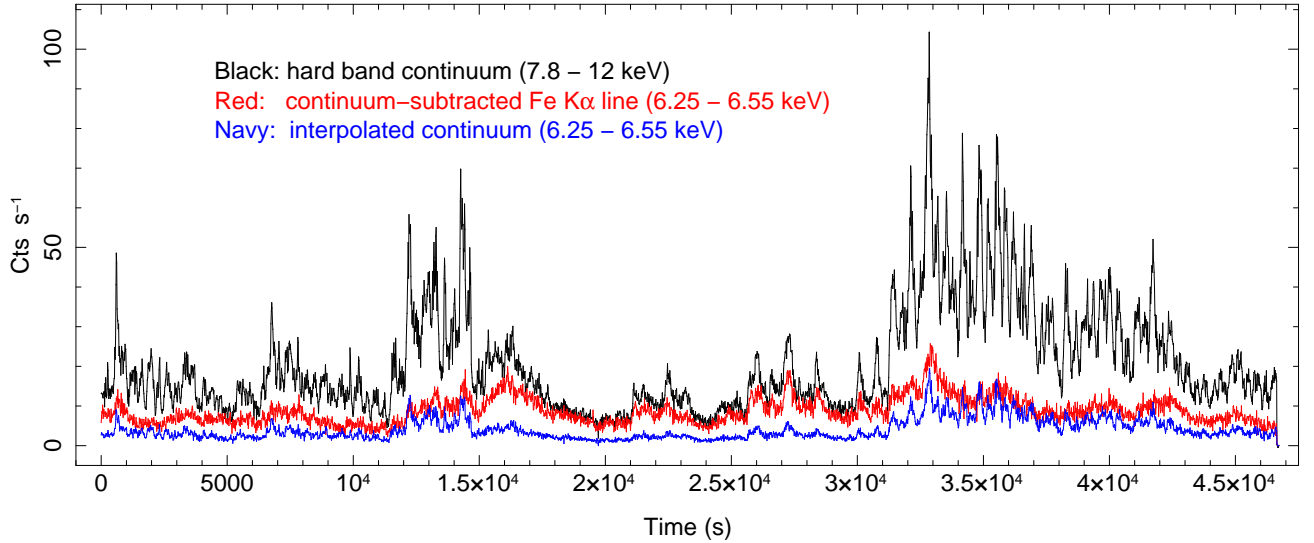


Figure 1. *XMM-Newton*/EPIC-pn light curves of GX 301-2 for the hard continuum (7.8–12 keV, black), the net Fe K α line (6.25–6.55 keV, red) and the interpolated continuum in the Fe K α band (6.25–6.55 keV, navy). They are binned in 10 s.

from a region smaller than the radius of the donor star (see [Martínez-Núñez et al. 2017](#), and references therein).

While for non-eclipsing SgXBs, it is generally hard to estimate their Fe K α -emitting region accurately. This is especially true for GX 301-2, the fluorescence region of which is of vigorous debate, although it shows one of the brightest Fe K α line among SgXBs. Using *ASCA* data of GX 301-2, [Endo et al. \(2002\)](#) measured a line width of 40–80 eV for the Fe K α line and inferred an emission region within $\sim 10^{10}$ cm (0.3 lt-s) from the neutron star. [Füerst et al. \(2011\)](#) investigated the cross-correlation between the continuum (7.3–8.5 keV) flux and the Fe K α line (6.3–6.5 keV) with *XMM-Newton* data, and could not find a significant time delay above 2 s, implying a distance smaller than 2 lt-s. They also proposed a second absorber on 2000 lt-s scale from an interval of low flux (lasted ~ 4.5 ks), during which the Fe K α line was clearly visible, while the continuum decreased significantly. By contrast, [Suchy et al. \(2012\)](#) inferred a distance greater than 700 lt-s, based on the flat pulse profile of the Fe K α line using *Suzaku* observations of GX 301-2. They attributed the lack of pulsation in the Fe K α line to the smearing effect of a large distance.

The absorption column density of GX 301-2 near periastron is quite high, $\sim 2 \times 10^{24}$ cm $^{-2}$ (e.g. [Füerst et al. 2011](#)). Such a high column density was also inferred from the Compton shoulder of the Fe K α line by [Watanabe et al. \(2003\)](#). The different estimations of the Fe K α -emitting region of GX 301-2 have a great impact on the gas distribution around the neutron star. For example, if the Fe K α -emitting region has a size scale ~ 1 lt-s, a density $\sim 7 \times 10^{13}$ cm $^{-3}$ is needed to provide the observed column density. This density is 1000 times higher than the local wind density, 6×10^{10} cm $^{-3}$, estimated from a mass-loss rate of 10^{-5} M $_{\odot}$ yr $^{-1}$ and a wind velocity of 150 km s $^{-1}$ at the location of the neutron star near periastron ([Kaper et al. 2006](#)). On the other hand, if the Fe K α -emitting region is larger than 700 lt-s, it implies that the Fe K α photons are mainly produced by some gas far away from the neutron star and the optical companion star (the periastron distance of GX

301-2 is only 200 lt-s). The densities of the stellar wind of GX 301-2 on such large scales is far below the observed high column density. Furthermore, the temporal correlation between the Fe K α line and the continuum, is apparently much shorter than 700 s (e.g. [Füerst et al. 2011](#), see also Figure 1 above).

We note that in the cross-correlation analysis done by [Füerst et al. \(2011\)](#), they used a time bin of 1 s, within which the average counts of the Fe K α photons are ~ 10 , and the Poisson noises could be significant. More importantly, they did not subtract the underlying continuum within the Fe K α band (6.3–6.5 keV), which, as illustrated in Figure 1, is significant. As shown in our analysis, whether subtracting the underlying continuum or not totally changes the behavior of the cross-correlation function. This motivates us to revisit the problem of the Fe K α -emitting region of GX 301-2 with the cross-correlation method, which was not regularly exploited when estimating the spatial distribution of the circumstellar material in SgXBs and could be potentially applied to a large number of SgXBs with future X-ray missions of large collecting area, such as Athena and eXTP.

In § 2 we describe the data used. § 3 presents the analysis and results. We discuss the implications of the results in § 4. All the errors in this paper are quoted for the confidence level of 90%.

2 OBSERVATION DATA

We use the same *XMM-Newton* dataset (Obs.ID 555200401) analysed in [Füerst et al. \(2011\)](#). The observation was carried out on 2009 July 12, with an exposure of 46 ks, using EPIC-pn in the timing mode. The timing mode allows observations of count rates up to 400 cts s $^{-1}$ without detectable pile-up. The corresponding orbital phases are ~ 0.98 , according to the ephemeris of [Doroshenko et al. \(2010\)](#) (~ 0.92 for the ephemeris of [Koh et al. \(1997\)](#)).

The data were reprocessed with the Science Analysis Software (SAS 17.0.0), following the standard procedures.

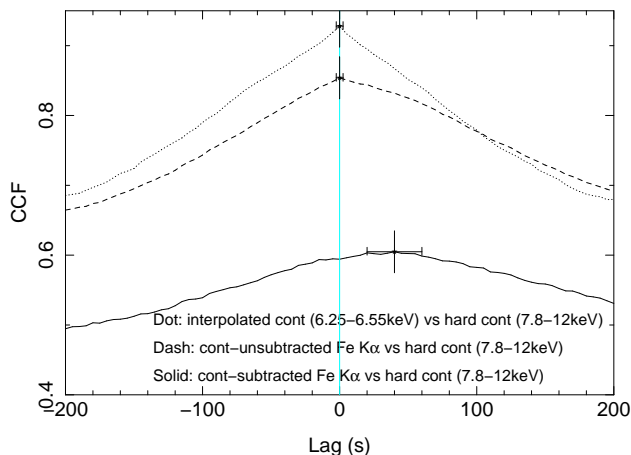


Figure 2. CCFs between the interpolated continuum, the unsubtracted Fe $K\alpha$ line, the net Fe $K\alpha$ line, and the hard continuum, respectively. The peaks of CCFs are showed with the vertical lines, and the error bars are estimated from re-sampling of the light curves. Subtraction of the underlying continuum is crucial to reveal the true time delay of the Fe $K\alpha$ line.

Compared with the data reduction in Fürst et al. (2011), the biggest difference is the application of a rate-dependent correction of energy scale in the Fe $K\alpha$ band for PN exposures in timing mode¹. Before filtering and extracting the high level products with *evselect*, the barycentric correction is applied via *fool barycen*, and the binary effect is corrected with the program *binaryCor* in *Remis* ISISscripts². The source data were extracted from Cols. 29–47 and the background data from Cols. 3–5.

3 ANALYSIS AND RESULTS

The extracted light curves of the hard continuum (7.8–12 keV) and the Fe $K\alpha$ line (6.25 – 6.55 keV) are presented in Figure 1. The energy range of 7.8 – 12 keV is chosen to exclude the contributions from Fe $K\beta$ and Ni $K\alpha$ lines. A baseline continuum for the Fe $K\alpha$ line is estimated from a linear interpolation between the rates within 5.7 – 6.1 keV and 6.7 – 6.9 keV, and is shown as the navy line in Figure 1. The hard continuum shows intense flares at the beginning (0–15 ks) and the ending (30–46 ks) of the observation, and stays relatively quiescent in the middle (15–30 ks). The Fe $K\alpha$ fluxes show good correlations with the hard continuum fluxes in the quiescent period, but not in the flare periods. The averaged rate of the interpolated baseline continuum of the Fe $K\alpha$ line is about 30% of that of the Fe $K\alpha$ line in the middle quiescent period, and is comparable to that of the Fe $K\alpha$ line during the flare periods. It illustrates the significant contribution of the underlying continuum to the observed Fe $K\alpha$ line.

As the Fe $K\alpha$ photons are emitted from the reprocessing of the intrinsic hard X-ray continuum of the neutron star by the surrounding material, a time delay of the Fe $K\alpha$ line

behind the hard continuum, corresponding to the average distance of the surrounding material to the neutron star, is expected. We apply the standard cross-correlation function (CCF) method (e.g. Peterson 1993) to measure the time delay. The CCF is defined as:

$$\text{CCF}(\tau) = \frac{\sum_t L_c(t - \tau) L_{\text{Fe}}(t)}{\sqrt{\sum_t L_c^2(t) \sum_t L_{\text{Fe}}^2(t)}} \quad (1)$$

where L_c and L_{Fe} are the light curves of the hard continuum and the Fe $K\alpha$ line, respectively. Both L_c and L_{Fe} are normalized by the root mean square of the light curves to ensure that the resulting CCF values are between -1 and 1.

3.1 CCFs for the whole observation

We calculated three CCFs with respect to the hard continuum (7.8 – 12 keV): for the interpolated continuum in the Fe $K\alpha$ band, the continuum-unsubtracted Fe $K\alpha$ line, and the continuum-subtracted Fe $K\alpha$ line, respectively. The light curves (with a binsize of 5 s) over the whole observation are summed. The resulting CCFs are presented in Figure 2. The CCF between the interpolated continuum and the hard continuum is peaked around 0 and shows a symmetric profile, indicating that they have almost no time delay. The CCF between the continuum-unsubtracted Fe $K\alpha$ line and the hard continuum is also peaked around 0, showing no significant time delay, as reported by Fürst et al. (2011). Note that its profile is a little skewed toward the positive side, which is an indication of a positive time delay (Peterson et al. 1998). The CCF between the continuum-subtracted Fe $K\alpha$ line and the hard continuum, however, is peaked around 40 s, and is also skewed toward the positive side. Therefore, the CCF between the continuum-unsubtracted Fe $K\alpha$ line and the hard continuum can be regarded as a combination of the CCFs of the interpolated continuum and the net Fe $K\alpha$ line with respect to the hard continuum. The interpolated underlying continuum dominates the location of the peak of the continuum-unsubtracted CCF (0 s), while the Fe $K\alpha$ line produces the skewness of the continuum-unsubtracted CCF. The time delay of the Fe $K\alpha$ line with respect to the hard continuum becomes obvious only when the underlying continuum is subtracted.

We estimated the measurement errors of the time delay by re-sampling the light curves of the Fe $K\alpha$ line and the hard continuum with a Poission distribution for 5000 times, and calculating the distribution of the peaks of sampled CCFs. We found a time delay of 40 ± 20 s.

3.2 CCFs for 15 ks periods

As discussed above, the hard continuum of GX 301-2 shows intense flares for the first 15 ks and the last 15 ks, and keeps quiescent in the middle, and the Fe $K\alpha$ fluxes are well correlated with the continuum fluxes in the middle quiescent period, but not in the flare periods. To study the dependence of the CCF on the flare activity, we divided the observation into three 15 ks periods and calculated the CCF between the continuum-subtracted Fe $K\alpha$ line and the hard continuum (7.8 – 12 keV), respectively. In order to obtain a stable CCF profile, the light curves are binned in 15 s. The resulting CCFs are plotted in Figure 3.

¹ <http://xmm2.esac.esa.int/docs/documents/CAL-SRN-0312-1-4.pdf>

² <http://www.sternwarte.uni-erlangen.de/isis>

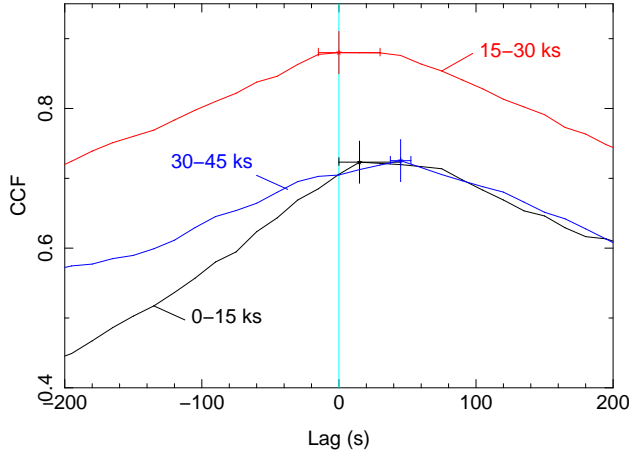


Figure 3. CCFs for three 15 ks periods. They indicate that the Fe $K\alpha$ -emitting region is varying.

The CCF of the middle quiescent period shows the highest correlation value, consistent with the apparent good correlation between the Fe $K\alpha$ fluxes and the hard continuum fluxes shown in Figure 1. The peak of the CCF of the middle 15ks period is located around 0_{-15}^{+30} s. The CCFs of the first 15 ks and the last 15 ks show a relatively low correlation value, and have positive peaks at 15_{-15}^{+30} s and 45 ± 7.5 s, respectively. Because the peaks of sampled CCFs of the last 15 ks are all located in one bin, half of the binsize 7.5 s is taken as the errors. The CCF profile of the first 15 ks shows a clear skewness towards the positive side. These results indicate that the Fe $K\alpha$ -emitting region is varying on a time-scale of 15 ks.

3.3 CCFs for 5 ks periods

To further study the variation of the Fe $K\alpha$ -emitting region, which implying an unsteady accretion flow around the neutron star, we further derived the three 15 ks periods into smaller time spans of 5 ks. The light curves are binned in 20 s. The resulting CCFs are plotted in Figure 4. Similar to the cases of 15 ks periods, most of the CCFs have a positive time delay in the range of 20–60 s. During the first 15 ks (the left panel), the intense flare within 10–15 ks stands out for its higher correlation value and apparent time lag of 60_{-40}^{+20} s. During the second 15 ks (the middle panel), the quiescent period of 15–20 ks shows the highest correlation value, and its profile is more spreading compared to other periods. During the last 15 ks (the right panel), the intense flare within 30–35 ks is also remarkable for its higher correlation value and prominent time lag of 40_{-10}^{+20} s. In general, the intense flare periods (10–15 ks and 30–35 ks) show the largest time delays, while the quiescent periods show smaller time delays.

4 DISCUSSION AND CONCLUSION

We studied the time delay between the Fe $K\alpha$ line and the hard continuum of GX 301-2 using the CCF method with *XMM-Newton* data. We found that the subtraction of the underlying continuum in the Fe $K\alpha$ band is crucial to reveal

the true time delay between the Fe $K\alpha$ line and the hard continuum. The measured time delay over the whole observation period is 40 ± 20 s. The measured time delay of the middle quiescent period (15–30 ks) is 0_{-15}^{+30} s, a little smaller than those of the flare periods (0–15 ks and 30–45 ks). The best measurements of positive time delays are from the intense flare periods of 10–15 ks and 30–35 ks, which are 60_{-40}^{+20} s and 40_{-10}^{+20} s, respectively. These results show that the typical Fe $K\alpha$ -emitting region of GX 301-2 is around 40 lt-s, and it can vary over the time-scale of 5–15 ks.

Our results are quite different from those reported previously for GX 301-2. Endo et al. (2002) inferred a smallest Fe $K\alpha$ -emitting region ~ 0.3 lt-s. It is most likely because they over-estimated the Fe $K\alpha$ line width due to the limited spectral resolution of *ASCA*. With a higher spectral resolution, *Chandra* HETG observation of GX 301-2 provided a Fe $K\alpha$ line width ~ 4 eV (e.g. Liu et al. 2018; Tzanavaris & Yaqoob 2018), indicating a much larger scale. Fürst et al. (2011) found no significant time delay beyond 2 s, which, as shown in the analysis of § 3, is because that the underlying continuum within the Fe $K\alpha$ band was not subtracted. They also identified a period of low state (lasting for ~ 4.5 ks) and inferred a second absorber on 2000 lt-s scale. The time delay during this low state (17–21 ks) is ~ 0 s, inconsistent with an emitting region of a large scale of 2000 lt-s. A possible scenario is that a thick gas structure temporarily obscured the intrinsic hard emission of the neutron star, and the observed hard continuum were mainly from scattered emission. To heavily obscure the photons of 7.8–12 keV, a column density larger than 2×10^{24} cm $^{-2}$ is required. In principle, the Fe $K\alpha$ -emitting gas itself could play the absorption role.

On the other hand, Suchy et al. (2012) inferred a scale larger than 700 lt-s based on the flat pulse profile of the Fe $K\alpha$ line. We note that as long as the fluorescence material is quasi-symmetric with respect to the rotational axis of the neutron star, the illuminating radiation on the fluorescence material will be similar for any spin phases, and the resulting Fe $K\alpha$ line will show no apparent pulsation. The fluorescence material is not necessarily to be as far as the light travel distance of spin period (685 lt-s) to destroy the coherence.

The circumstellar material will be gravitationally bounded by the neutron star if it is within the accretion radius:

$$R_{\text{acc}} = \frac{2GM}{v_{\text{rel}}^2} \simeq 55 \frac{M}{1.4 M_{\odot}} \left(\frac{v_{\text{rel}}}{150 \text{ km s}^{-1}} \right)^{-2} \text{ lt-s}, \quad (2)$$

where $v_{\text{rel}} = \sqrt{v_{\text{orb}}^2 + v_{\text{w}}^2}$ is the relative velocity of the neutral star with respect to the surrounding material, v_{orb} is the orbital velocity, and v_{w} is the wind velocity at the location of the neutron star. $v_{\text{orb}} \sim 350$ km s $^{-1}$ and $v_{\text{w}} \sim 150$ km s $^{-1}$ near the periastron adopting the orbit parameters of Doroshenko et al. (2010) and a terminal velocity of 400 km s $^{-1}$. These values provide an accretion radius $R_{\text{acc}} \sim 8$ lt-s, 5 times less than the measured average size of Fe $K\alpha$ -emitting region.

A very particular aspect of GX 301-2 is that it shows pre-periastron X-ray flares around orbital phases ~ 0.92 (e.g. Leahy 2002; Islam & Paul 2014). It could be explained by an accretion stream originating from the surface of the donor star (Leahy & Kostka 2008). They inferred that the stream has a mass-loss rate 2-3 times larger than that of the

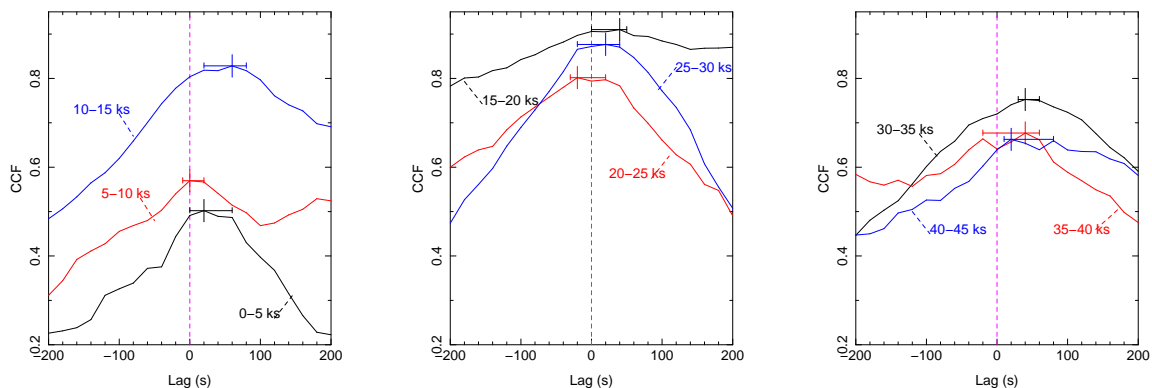


Figure 4. CCFs for 5 ks periods in 20 s resolution. The vertical lines represent the peaks. Left: 0-5, 5-10, 10-15 ks; Middle: 15-20, 20-25, 25-30 ks; Right: 30-35, 35-40, 40-45 ks.

stellar wind. Thus the stream could be the dominate mass-loss mechanism of the massive star of GX 301-2. Evidences for the existence of the stream are also found in the studies of optical lines (Kaper et al. 2006) and mid-infrared interferometry (Waisberg et al. 2017). If the accretion stream is indeed the dominant mass-loss mechanism, the neutron star is passing the stream near the periastron, and the relative velocity between the stream and the neutron star in the orbital direction will be small. In this case, $R_{\text{acc}} \sim 55$ lt-s, similar to the measured average size of Fe $K\alpha$ -emitting region. Since R_{acc} is a natural physical scale for the distribution of the circumstellar material, the measured Fe $K\alpha$ -emitting region favours the case of the accretion stream, rather than the quasi-isotropic stellar wind.

It is very interesting to note that the measured sizes of Fe $K\alpha$ -emitting region on time-scales of 5-15 ks are variable, changing from a larger scale during the intense flares, to a smaller scale for the quiescent periods. Such a behavior is consistent with the unsteady nature of the accretion flow in wind-fed systems, as illustrated in numerical simulations (e.g. Taam & Fryxell 1988; Blondin et al. 1990, among others). A change of 10 lt-s on time-scales of 10 ks implies a velocity of 300 km s^{-1} , which is physically plausible. The significance of the unsteady behaviour of the Fe $K\alpha$ -emitting material is limited by the current observation data, and further observations of GX 301-2 will help to improve the significance and to probe the unsteady evolution of the circumstellar material on longer time-scales.

In conclusion, these results show that the spatial distribution of the circumstellar material of GX 301-2 can be measured from the time delay between the Fe $K\alpha$ line and the hard continuum using CCF method. This methodology might be applicable to other few SgXBs with bright Fe $K\alpha$ lines using archival data, and will be explored in a future work. The available candidates would be limited to few bright sources. Nevertheless, with future X-ray missions of larger collecting area, such as Athena and eXTP, much more SgXBs would be available to be studied using the CCF method, as illustrated here. Statistical studies of the circumstellar material with other properties in these systems, such as wind velocities, are expected. The unsteady behaviour of the accretion flow in such systems will be better revealed, and its correlation with other properties, such as the observed fluxes, will be studied in great details.

ACKNOWLEDGEMENTS

JL acknowledges the support by National Natural Science Foundation of China (NSFC, 11773035). LG acknowledges the supported by the National Program on Key Research and Development Project through grant No. 2016YFA0400804, and by the National NSFC with grant No. Y913041V01, and by the Strategic Priority Research Program of the Chinese Academy of Sciences through grant No. XDB23040100. This work has also made use of the archive data from the XMM-Newton, an ESA science mission funded by ESA Member States and USA (NASA).

REFERENCES

- Blondin J. M., Kallman T. R., Fryxell B. A., Taam R. E., 1990, *ApJ*, **356**, 591
- Davidson K., Ostriker J. P., 1973, *ApJ*, **179**, 585
- Doroshenko V., Santangelo A., Suleimanov V., Kreykenbohm I., Staubert R., Ferrigno C., Klochov D., 2010, *A&A*, **515**, A10
- Endo T., Ishida M., Masai K., Kunieda H., Inoue H., Nagase F., 2002, *ApJ*, **574**, 879
- Fürst F., et al., 2011, *A&A*, **535**, A9
- Giménez-García A., Torrejón J. M., Eikmann W., Martínez-Núñez S., Oskinova L. M., Rodes-Roca J. J., Bernabéu G., 2015, *A&A*, **576**, A108
- Haberl F., White N. E., Kallman T. R., 1989, *ApJ*, **343**, 409
- Islam N., Paul B., 2014, *MNRAS*, **441**, 2539
- Kaper L., van der Meer A., Najjarro F., 2006, *A&A*, **457**, 595
- Koh D. T., et al., 1997, *ApJ*, **479**, 933
- Leahy D. A., 2002, *A&A*, **391**, 219
- Leahy D. A., Kostka M., 2008, *MNRAS*, **384**, 747
- Liu J., Soria R., Qiao E., Liu J., 2018, *MNRAS*, **480**, 4746
- Martínez-Núñez S., et al., 2017, *Space Sci. Rev.*, **212**, 59
- Nagase F., 1989, *PASJ*, **41**, 1
- Peterson B. M., 1993, *PASP*, **105**, 247
- Peterson B. M., Wanders I., Horne K., Collier S., Alexander T., Kaspi S., Maoz D., 1998, *PASP*, **110**, 660
- Suchy S., Fürst F., Pottschmidt K., Caballero I., Kreykenbohm I., Wilms J., Markowitz A., Rothschild R. E., 2012, *ApJ*, **745**, 124
- Taam R. E., Fryxell B. A., 1988, *ApJ*, **327**, L73
- Torrejón J. M., Schulz N. S., Nowak M. A., Kallman T. R., 2010, *ApJ*, **715**, 947
- Tzanavaris P., Yaqoob T., 2018, *ApJ*, **855**, 25
- Waisberg I., et al., 2017, *ApJ*, **844**, 72
- Watanabe S., et al., 2003, *ApJ*, **597**, L37

This paper has been typeset from a \TeX/L\AA\TeX file prepared by the author.